

# Electronics of a Wearable ECG With Level Crossing Sampling and Human Body Communication

Jinxi Xiang , *Student Member, IEEE*, Yonggui Dong , Xiaohui Xue, and Hao Xiong

**Abstract**—In this paper, the human body communication (HBC) and level crossing sampling (LCS) are combined to design electronics for a wearable electrocardiograph (ECG). The ECG signals acquired by capacitively coupled electrodes are sampled with LCS in place of conventional synchronous sampling. In order to transmit signals through HBC at low frequencies (100 kHz, 1 MHz), an electric field sensor with high input impedance is adopted as the front end of the HBC receiver. The HBC channel gain is enhanced by more than 30 dB with the electric field sensor. An LCS structure based on the send-on-delta concept is implemented with discrete components to convert the ECG signals into binary impulses. The converted impulses are modulated by an on-off keying modulator and then transmitted via the human body to the receiver. A prototype ECG waist belt is developed with commercially available components and experimentally evaluated. The results indicate that the acquired ECG waveforms exhibit good agreement with regular Ag/AgCl ECG methods. The heartbeat detection using a technique based on the Kadane’s algorithm and the power consumption performance of the proposed system are also discussed.

**Index Terms**—Human body communication (HBC), level crossing sampling (LCS), wearable electrocardiograph (ECG).

## I. INTRODUCTION

WEARABLE sensors are becoming extremely popular because they allow ubiquitous sensing as part of daily life. Compared with other approaches, the close placement of the wearable sensors on the human body allows capturing high-quality signals [1]. By integrating them into fashion accessories or skin electronics, wearable sensors can be used for continuously monitoring health status in a highly unobtrusive way. This is especially true when the sensors are used to construct a Body sensor network (BSN) with Human Body Communication (HBC). Various wearable vital sign sensors are attached to the human body to collect physiological signals. All the sensors are capable of transmitting data via HBC which is a wireless communication scheme that exchanges information on the human

Manuscript received July 9, 2018; revised September 5, 2018 and October 21, 2018; accepted October 31, 2018. Date of publication November 6, 2018; date of current version January 25, 2019. This work was supported by the National Natural Science Foundation of China (no. 61671270). This paper was recommended by Associate Editor D. Gangopadhyay. (*Corresponding author: Yonggui Dong*)

The authors are with the State Key Laboratory of Precision Measurement Technology and Instruments, Department of Precision Instrument, Tsinghua University, Beijing 100084, China (e-mail: xiang\_jinxi@qq.com; dongyg@mail.tsinghua.edu.cn; xxh17@mails.tsinghua.edu.cn; tsinghua\_xionghao@126.com).

Color versions of one or more of the figures in this paper are available online at <http://ieeexplore.ieee.org>.

Digital Object Identifier 10.1109/TBCAS.2018.2879818

body through near-field propagation. At the wearable HBC hub, the HBC data from all sensors are aggregated.

HBC employs the human body as the communication channel. The data are transmitted and received between wearable sensors through near field propagation. HBC is a promising technology in BSN because, on the one hand, it does not require wires to interconnect sensors. It is convenient to set up or remove sensors and also enhances wearing comfort. On the other hand, HBC has good near-field transmission characteristics on the human body. Most of the HBC signals are confined to the body area without interference from external RF devices [2]. Moreover, the communication frequency of HBC, usually from tens of kilohertz to tens of megahertz, is much lower than typical 2.4 GHz wireless techniques like Bluetooth or ZigBee [3]. Therefore, HBC can reduce radiation dissipation.

The operation frequency of HBC is a paramount design consideration. For wideband signaling, it directly couples the non-return-to-zero (NRZ) digital signal into the human body without modulation. This scheme makes it easier to implement a compact system-on-a-chip HBC at 5 Mb/s [4] or a fast commercial-off-the-shelf (COTS) HBC prototype at 500 Kb/s [5] because without modulation and demodulation units, the transceiver is simplified. Another category is modulation methods using high frequencies carriers. Reference [6] reported a biomedical system-on-a-chip for HBC. The system operates at up to 145 MHz with on-off keying (OOK). In [3], capacitive HBC with impulse modulation between 10 and 60 MHz was achieved to develop a wearable ECG. Moreover, HBC is also adopted for biometric verification at frequencies from 650 MHz to 750 MHz because HBC signals are mainly confined within the human body that promises physically secure communication [2]. However, since the human body acts as an antenna between 40 ~ 400 MHz, it is susceptible to significant interference especially to the FM radio band (88 MHz ~ 108 MHz) [7]. Generally, in these studies, Ag/AgCl electrodes [6] or metallic electrodes [3] are chosen for transmission or receiving by direct contact with the skin. These electrodes have low input impedance and low sensitivity, resulting in insufficient pick-up amplification of HBC signals at low frequencies. Therefore, frequencies under 1 MHz are rarely investigated in capacitive HBC.

For BSN, another problem is the increasing data amount with the accumulation of time and the increase in the number of sensors. Therefore, data compression is a great concern in BSN. Many state-of-the-art algorithms for data compression are based on discrete wavelet transform (DWT) because of their straightforward implementation and effective compression performance

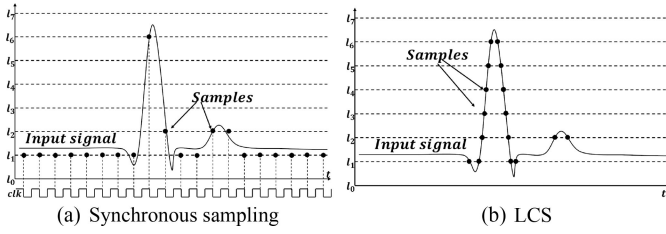


Fig. 1. Comparison between synchronous sampling and LCS.

[8]. However, data still need to be sampled at the Nyquist rate and stored in memory before they are compressed, which require extra power and storage capacity. Compressed sensing (CS) is an emerging technique that can lower the sampling rate greatly. Data are not required to be stored before being compressed. CS can achieve high compression ratios with low processing complexity when using a sparse binary matrix during sampling [9]. Unfortunately, the signal reconstruction processes involve algorithms with relatively high computational costs. Reconstructing long-term records can take a long time and high computing resources at embedded system [10]. Therefore, the complex post-processing for reconstruction is not applicable to wearable devices [11]. It is usually carried out on a computer as in [10]. Other legacy techniques like adaptive sampling [12] adjust the converter clock to reduce sample data volume. Although it generates fewer samples than a typical Nyquist sampler, the errors resulting from interpolation may cause conversion error so it could miss certain key features of the input signal.

The level crossing sampling (LCS) [13] provides another solution to significantly reduce the data amount for sparse and burst-like signals. In biomedical applications, signals are generally sparse [9], alternating long low-activity periods and short informative events. Examples of short informative events include the QRS complex of ECG, muscle contraction potentials of EMG, or neural action potentials (spikes) of EEG. Contrary to synchronous sampling triggered by a constant time interval (Fig. 1a), in level-crossing sampling (Fig. 1b), samples are generated only when the input signal crosses the quantization levels. The number of samples automatically correlated with the features of the input signal. Recently, level-crossing sampling has been considered in wearable devices by a growing number of researchers [11], [13]–[16]. For example, QRS detection using level crossing sampled data has been reported in [11]. The reference [16] has proposed an event-correlated scheme that has adaptive resolution and is totally clockless. It needs embedded memory which remembers the previous digital output values and the output are amplitude-time data pairs.

In this study, low frequencies (e.g. 100 kHz and 1 MHz) are chosen to avoid antenna effect of the human body as well as to reduce propagation power. To complement path loss due to low carrier frequency, an electric field sensor is used to detect HBC electric field. The main focus of this work is the development of hardware prototype of a wearable ECG system based on LCS and HBC, which is designed for non-clinical usages on a daily basis. Examples include ECG chest band [17], noncontact ECG armband [18], and HBC-ECG [3] for vehicle drivers. The key contributions of this paper are listed hereafter.

- Capacitive HBC is used for wireless transmission on the human body. The HBC operates at low frequencies (e.g. 100 kHz and 1 MHz) so as to minimize propagation power and interference. The human body channel is enhanced by electric field electrode with high input impedance and high gain over 30 dB.
- LCS is implemented with basic discrete components for signal sampling. It is a fixed resolution LCS scheme that needs clock but without embedded memory. It only generates impulses output and retrieves time information with synchronizer at the receiver.
- A novel framework combining HBC with LCS for body sensor network is demonstrated with commercial-off-the-shelf (COTS) components.

Section II proposes the HBC channel enhancement method with electric field sensor as well as a new LCS structure implemented with discrete components. Section III describes the overall structure of the wearable ECG belt based on the proposed HBC and LCS in Section II. To detect the R-peaks of ECG signals, a technique adapted from the Kadane's algorithm is also introduced in this section. Section IV evaluates the system performance. The ECG quality and R-peaks detection performance are analyzed and the power consumption is also discussed. Section IV concludes the whole study.

## II. HUMAN BODY COMMUNICATION AND LEVEL CROSSING SAMPLING

### A. Capacitive HBC with Electric Filed Sensor

As indicated in [19], the human body channel acts as a high pass filter under 4 MHz due to the capacitive return path, so the transmission frequency must be high enough to form a stable return path. Although data transmission with a high-frequency carrier can exploit the strong return path, it should not be excessively high because of the body antenna effect and power consumption problems. It is a common choice to select tens of megahertz for communication, as introduced in Section I. To our knowledge, until now, frequencies lower than 1 MHz are rarely investigated because of the extraordinarily high path loss at this range. For example, reference [7] reported around 40 dB loss at 17 cm distance from 10 kHz to 500 kHz. Reference [20] reported more than 50 dB loss at 140 cm distance for frequencies lower than 1 MHz. These research generally employed Ag/AgCl or metallic electrodes to receive the weak HBC signals. Such kinds of electrodes are simple and readily available but have low input impedance and small gain, making them vulnerable to noise for HBC communication especially when the path loss is high. Maity *et al.* [21] experimentally found that high-impedance receiver (1 MΩ oscilloscope) along with voltage-mode communication can maximize HBC received signal. This enlightens new way of designing high-sensitivity HBC electrode with high input impedance.

To address this problem, we utilize a high-sensitivity electric field sensor to receive HBC signal so as to enhance the HBC channel gain at low frequencies from 100 kHz to 1 MHz. The electrode is built on a 4-layer PCB structure which is of the similar design with the ECG sensing electrodes [17], [22]. Fig. 2

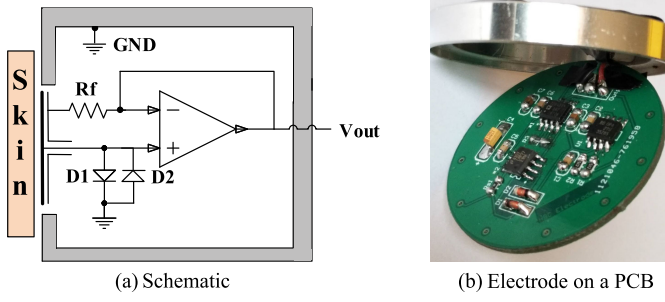


Fig. 2. Electric field sensor.

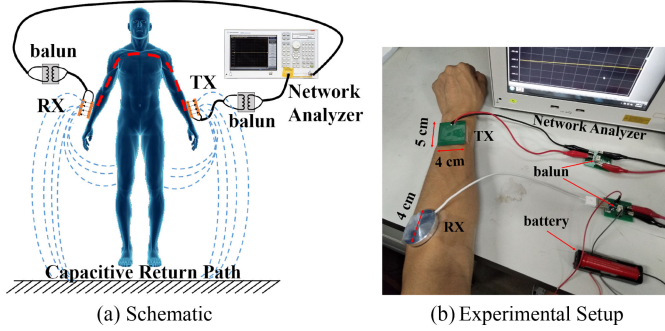


Fig. 3. HBC channel test.

shows the schematic and the PCB realization of the electrode. The front-end amplifier is required to buffer the signals from the body whilst introducing a minimum of noise. We use a wide-band amplifier AD8421 which has extremely low input current noise of  $200 \text{ fA}/\sqrt{\text{Hz}}$ , and high input impedance of  $30 \text{ G}\Omega$ . The schematic in Fig. 2 a is a simplified representation of configuring the AD8421 as a unity-gain amplifier. The amplification and the sensing electrode are built on one PCB by using the bottom copper as the sensing plane. This design can not only minimizes extraneously induced noise but also make more effective shielding. Due to the high impedance skin-electrode interface, the electric field sensor can be very sensitive to environmental noise. Active shielding is necessary to minimize environmental noise pick-up and reduce parasitic capacitance. Specifically, a guard ring around the input pin, the inner layers of the four-layer PCB and the metal cage surrounding the electrode are actively driven by the output of the front-end amplifier. The input sensitivity is proportional to the input impedance  $V_{OUT} = R_{IN} I$ . The proposed electric field sensor can achieve  $1 \text{ V/pA}$  sensitivity with elaborate design [22].

To test the HBC channel enhancement with an electric field sensor, experiment was carried out with a Network Analyzer Agilent-E5061B (Fig. 3). A balun (Mini-Circuit ADT1-6T+) with a 1:1 turns ratio is connected between the analyzer and the transmitter/receiver electrodes to separate the ground electrode from the ground of analyzer. The signal path thus is approximately the actual capacitive return path. The transmitter (TX) electrode is made up of 2-layer PCB in size of  $4 \text{ cm} \times 5 \text{ cm}$ . The top layer and the bottom layer serve as signal and ground electrode respectively. The receiver electrode (RX) is circular with a diameter of 4 cm (Fig. 3b). During the test, the TX and

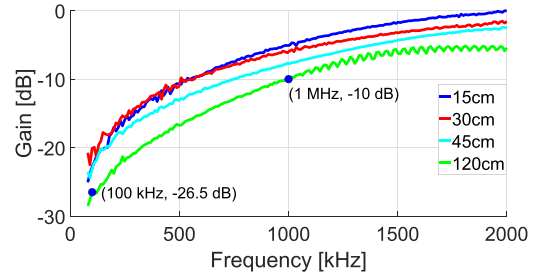


Fig. 4. HBC path loss at different distances (measured).

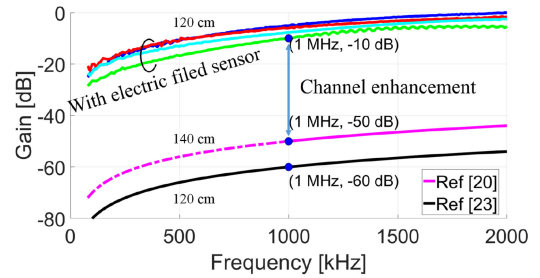


Fig. 5. HBC channel enhancement with electric field sensor (measured).

RX electrodes were moved along the arm from the subject's left to the right wrist at different distances.

The results of HBC channel test on the same person are presented in Fig. 4. Compared to the reported studies which use Ag/AgCl or metallic electrodes, there is a significant enhancement in the HBC channel (Fig. 5). The HBC channel gain is  $-10 \text{ dB}$  (120 cm) at 1 MHz, greatly enhanced from  $-50 \text{ dB}$  (140 cm) in [20] or  $-60 \text{ dB}$  (120 cm) in [23]. Data between 100 kHz to 1 MHz are not presented in ref [20], but we can derive from the HBC model. The characteristics of path loss are relatively deterministic with a slope of 20 dB/decade regardless of the distance because in the low frequency, the electric field is relatively constant throughout the whole human body. This result is in accordance with the analytical conclusion of [19] as well as the experimental results of [23]. From the observations above, it can be seen that the effect of electric field sensor is compensating the path loss of HBC and ensuring signal-to-noise ratio (SNR) in the meantime. Similar experiment results have also been reported by Maity *et al.* [21] which demonstrated that more than 10 dB HBC channel enhancement was achieved using  $1 \text{ M}\Omega$  oscilloscope compared with using  $50 \text{ }\Omega$  network analyzer. One primary explanation for the channel enhancement is using an impedance network model. Based on the voltage divider principle, extremely low path loss could be observed with a high input impedance load at the receiver termination [21].

Fig. 6 shows the HBC path loss variations of individual differences at 120 cm distance. It can be seen that the characteristics obtained for 4 different subjects differ less than 3 dB.

Fig. 7 plots the received signals at 1 MHz, 500 kHz, and 100 kHz as demonstrations examples. Signals at different frequencies are aligned and normalized on the time axis to gain clear illustrations. For higher frequencies, both the amplitude and the SNR of received signals are larger. Although there are noise and distortions, narrow-band digital transmission schemes

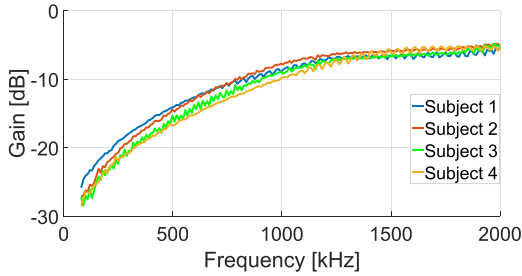


Fig. 6. HBC path loss at 120 cm distance for different subjects (measured).

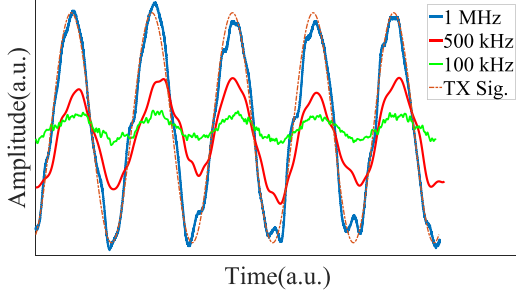


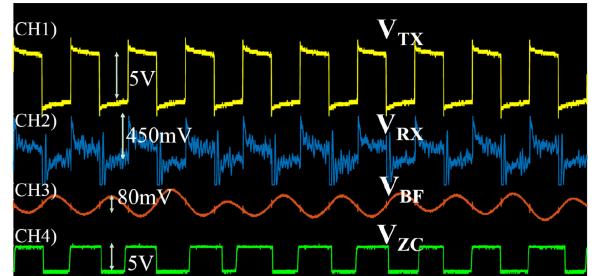
Fig. 7. HBC transmission characteristics with sine wave at 120 cm. Signals are aligned and normalized on the time axis. (measured).

can filter out the out-of-band spectral components efficiently. As the operation frequency increases, the HBC channel gain increases correspondingly. The front-end amplifier AD8421 of the electric field sensor has 10 MHz bandwidth ( $G = 10$ ). Thus, frequency above 100 kHz and under 10 MHz are all applicable to the proposed HBC electric filed sensor. In the experiment, we use OOK with two carriers at 100 kHz and 1 MHz to verify the feasibility of HBC at low frequency.

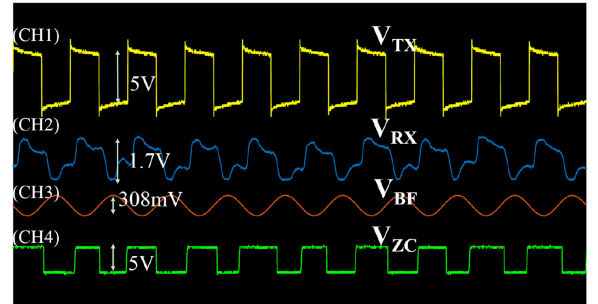
Two carrier waves were applied by signal generator to observe the transmission characteristics with an oscilloscope. There are 4 test points on the transmission path: (CH1) output of the transmitter (VTX); (CH2) received signal with electric field sensor (VRX); (CH3) filtered signal with band pass filter; (CH4) restored signals after comparator. Fig. 8 shows the measured signal characteristics. In both cases, although the received waves suffer from distortions, they can be recovered with bandpass filters that remove most wide-band noise and comparator that restores signals to logic level.

We also tested capacitive HBC for different body positions. The results demonstrated that the variations of the body position affect the HBC channel gain less than 2 dB (data not shown). This conclusion is consistent with the reported research [23]. The transmission characteristics are relatively stable for different body positions in the whole frequency range.

In comparison, Ag/AgCl electrodes are readily available and cheap. Electric field sensors are more complicated because they utilize front-end amplifiers with high input impedance and wide bandwidth. Elaborate design in shielding and PCB layout are also required to guarantee SNR. Since electric field sensors acquire signals capacitively, they are more sensitive to the displacement of the skin-electrode interface. Ag/AgCl electrodes are less affected by the skin-electrode movements because they have adhesive direct contact with the skin.



(a) 100 kHz



(b) 1 MHz

Fig. 8. HBC transmission characteristics with square wave at 120 cm (measured).

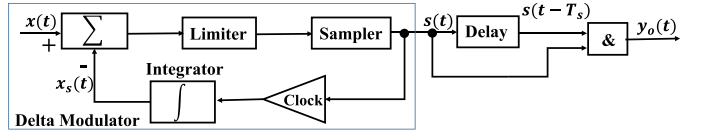


Fig. 9. The uLCS block diagram.

### B. Level Crossing Sampling

The basic circuit of the level-crossing sampling (LCS), called as upward level-crossing sampling (uLCS), is designed based on the send-on-delta concept as in [24]. The uLCS is sensitive to the incremental parts of the input signal. As shown in Fig. 9, it comprises a delta modulator and a delay unit. In the delta modulator, a negative feedback loop is formed to convert the input analog signal  $x(t)$  to binary impulses  $s(t)$ . After delayed for one sampling interval  $T_s$ , the delayed  $s(t - T_s)$  is taken to do Boolean AND operation with  $s(t)$ , yielding the binary output samples  $y_o(t)$ .

The operational principle of the uLCS is shown in Fig. 10. The input signal  $x(t)$  is converted into binary impulses  $s(t)$  with delta modulation. After being delayed and doing Boolean AND operation, the impulses corresponding to inactive signal segments are eliminated, and only impulses corresponding to the rising edge segments are retained (Fig. 10). This can remove the sparse impulses produced by DC or nearly DC signals such as the baseline drift in ECG signals.

The hardware circuit of the uLCS is shown in Fig. 11. The circuit makes use of a comparator, a D-type flip-flop, an analog switch, and an integrator to set up the negative feedback loop. The D-type flip-flop and the AND gate are used to implement a differentiator. Fig. 12 gives an example of the uLCS results (blue curve) of one simulated ECG signal (red curve). The sampling

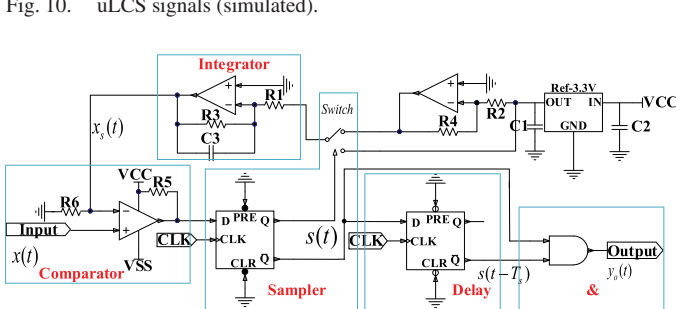
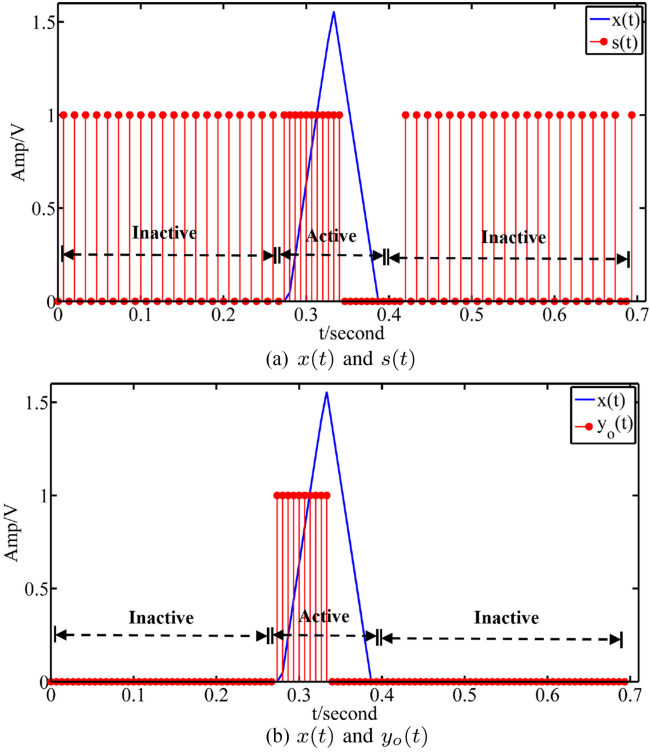


Fig. 11. uLCS schematic.

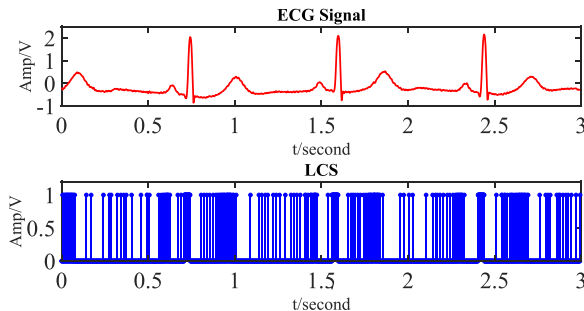


Fig. 12. uLCS results (simulated).

clock (CLK in Fig. 11) is provided by a NOT gate oscillator locally.

Since the uLCS is only sensitive to the incremental parts of the input signal, the downward LCS (dLCS), which is sensitive to the decremental parts of the input signal, is achieved by inverting the input signal as Fig. 13. The outputs of uLCS and the dLCS are combined in parallel to construct the complete

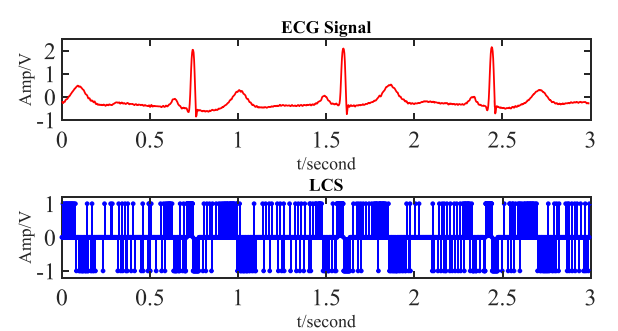
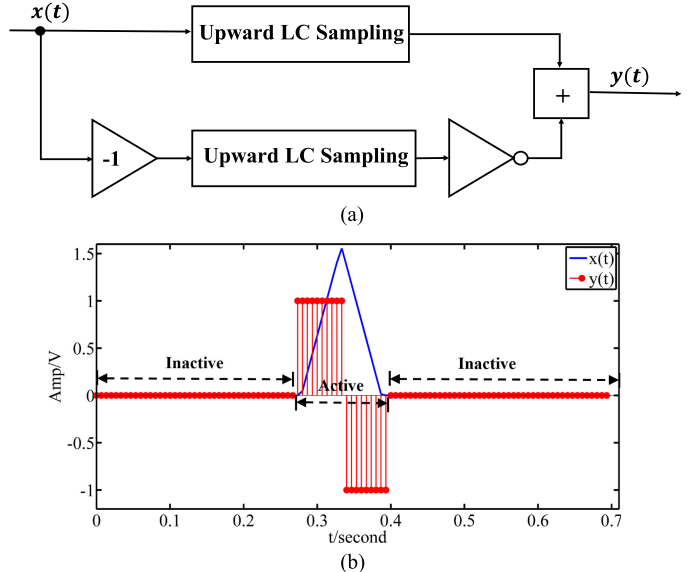


Fig. 14. The complete LCS results (blue curve) of one ECG signal (red curve).

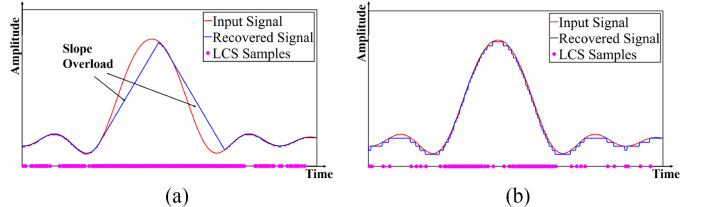


Fig. 15. LCS with (a) smaller  $\Delta$ , (b) appropriate  $\Delta$  (simulated).

LCS output  $y(t)$  in Fig. 13(b), where  $+1$  denotes that the input signal crosses the quantization levels upwards,  $-1$  downwards and  $0$  denotes that the signal does not cross any quantization levels. Fig. 14 illustrates a measurement example of the complete LCS results (blue curve) of an ECG signal (red curve). The quantification errors introduced by level crossing sampler have been theoretically analyzed by [15].

The resolution  $\Delta$  of the proposed LCS scheme is an important parameter. Fig. 15 shows two cases of  $\Delta$  for a given input signal. The output samples of the LCS are indicated by the dot marks on the horizontal time axis. In Fig. 15(a), when the input signal varies with a relatively lower slope rate, the LCS samples can track the input perfectly. However, when the input signal varies with higher slope rate, the LCS samples cannot track the signal,

TABLE I  
COMPONENT LIST OF FIG. 11

Component	Value	Component	Value
$R_1$	50 kΩ	$R_2$	1 kΩ
$R_3$	50 kΩ	$R_4$	1 kΩ
$R_5$	4.7 kΩ	$R_6$	3.3 kΩ
$C_1$	0.1 μF	$C_2$	0.1 μF
$C_3$	3.3 μF	comparator	LM311
D Flip Flop	CD4013	AND Gate	CD4081
Op. Amp.	OPA227	Ref-3.3	LM1117-3.3

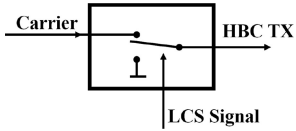


Fig. 16. OOK modulator.

resulting in slope overload. The slope of the input signal is limited to

$$\frac{\Delta}{T_s} \geq \left| \frac{dx(t)}{dt} \right|_{\max} \quad (1)$$

As indicated by (1), when  $T_s$  is constant,  $\Delta$  determines the maximum slew rate range of the input signal. Larger  $\Delta$  can accept higher slew rate, but would result in lower resolution. Therefore,  $\Delta$  is set to the minimum value that can meet the maximum slew rate of the input signal in (1), as shown in Fig. 15(b). In the circuits of Fig. 11,  $\Delta$  is adjusted by

$$\Delta = \frac{V_{ref}}{\tau f_s} = \frac{V_{ref}}{R_1 C_3 f_s} \quad (2)$$

where  $V_{ref}$  is provided by a voltage reference chip and  $\tau$  is the constant of integration determined by  $R_1 C_3$ . For example, for an ECG signal with a peak-to-peak amplitude of 700 mV and a maximum slope of 17 V/s, we set  $R_1 = 50 \text{ k}\Omega$ ,  $C_3 = 3.3 \mu\text{F}$ ,  $f_s = 15 \text{ kHz}$ ,  $V_{ref} = 3.3 \text{ V}$ . The resolution  $\Delta = 1.33 \text{ mV}$ , which also satisfies (1).

### C. Communication Transceiver

**HBC transmitter.** An OOK modulator is utilized to modulate the  $y(t)$  into higher frequency domain that is suitable to be transmitted via human body channel. As shown in Fig. 14, since the sampled LCS signal contains both upward sampling and downward sampling, which correspond to +1 and -1 respectively, two carrier signals of 100 kHz and 1 MHz are used for uLCS modulation and dLCS modulation respectively.

**HBC receiver.** The block diagram of the HBC receiver is shown in Fig. 17. The signal from the receiver electrode is amplified and filtered by two parallel band-pass filters with center frequencies of 100 kHz and 1 MHz respectively (Fig. 18). The comparator in Fig. 18 restores the filtered signals to logic level. The uLCS and dLCS binary codes are then obtained by the OOK demodulators which is configured with a phase lock loop (PLL) chip CD4046. Two output ports are designed in our prototype receiver. Output 1 is uLCS binary impulse sequence

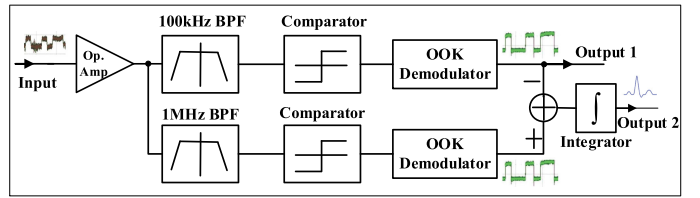


Fig. 17. Block diagram of the HBC receiver.

that can be used directly for R-peaks detection (see details in Section II.C). Output 2 is the recovered ECG signals after the integration of the LCS.

Fig. 19 is a snapshot of the received signal (yellow curve), the OOK demodulator output (blue curve), and the recovered ECG signal (violet curve), respectively.

Careful considerations should be given to the implementation of HBC. The circuit is vulnerable to interference especially when the ECG acquisition module and the HBC transmission module are mounted on the same board. One of our strategies is isolating the ECG acquisition circuit and the HBC transmitter with an isolation amplifier. Another strategy is reducing the working frequency of HBC. Compared to the commonly used frequencies up to tens of megahertz, we lower the frequency to 100 kHz and 1 MHz while ensuring the SNR of HBC signals by using high-sensitivity sensor. This electrode employs active shielding to depress parasitic capacitance and guard ring to construct a complete Faraday cage to improve interference reduction.

### III. IMPLEMENTATION OF THE PROPOSED SYSTEM

We demonstrate the proposed LCS and HBC based BSN with only the ECG sensor as an example. The proposed wearable ECG waist belt, as shown in Fig. 20, consists of an ECG acquisition module, an HBC transmitter, and an HBC receiver. In the ECG acquisition module, the ECG signals are acquired on the abdomen with two capacitively-coupled ECG sensing electrodes fabricated in the four-layer printed circuit boards (PCBs) [17], [22]. A ground electrode is attached to the abdomen skin as a reference. The ECG signal is acquired capacitively with electric field sensors. Therefore, DC offset is less of concerns in signal source. The DC offset caused by the input bias current of amplifiers is further mitigated by the use of a high-pass filter. The output signals from the ECG sensing electrodes are differentially amplified to depress the common-mode noise. After being filtered by the bandpass filter and notch filter, the ECG signal is sampled with level-crossing sampling and then modulated by on-off keying (OOK) with a 100-kHz carrier and a 1-MHz carrier. The modulated signals are capacitively coupled into the human body with a copper electrode.

The HBC receiver in Fig. 20 represents a simplified schematic. The entire hardware configuration of the receiver is illustrated in Fig. 18 with all the connection details and chip selections. The first stage of the HBC receiver denoted as Op. Amp. is the HBC receiver electrode that is described in Fig. 2. HBC signals are received with an electric field sensor capacitively from the human hand. The received signals are recovered

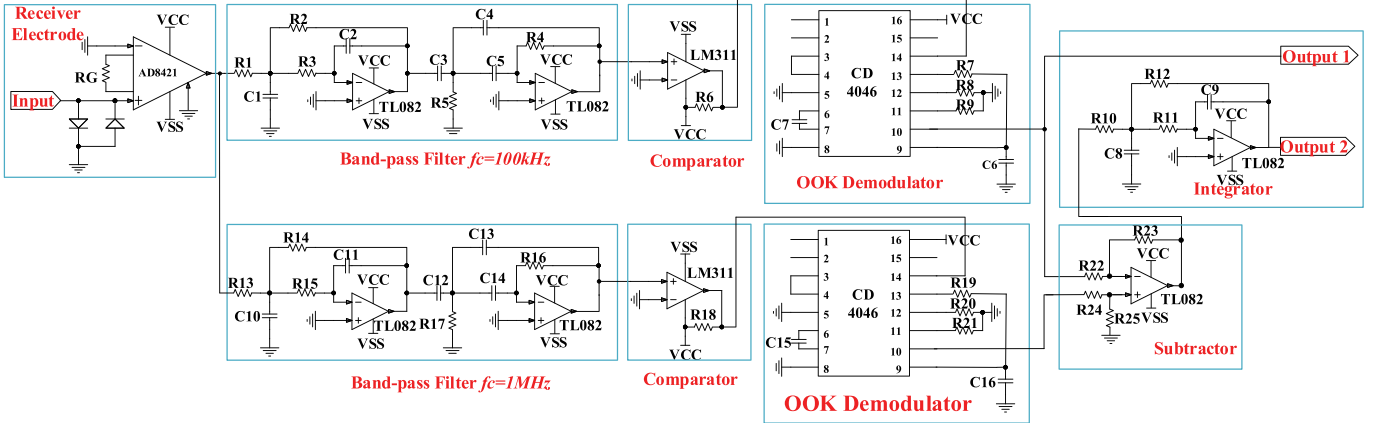


Fig. 18. HCB receiver schematic.

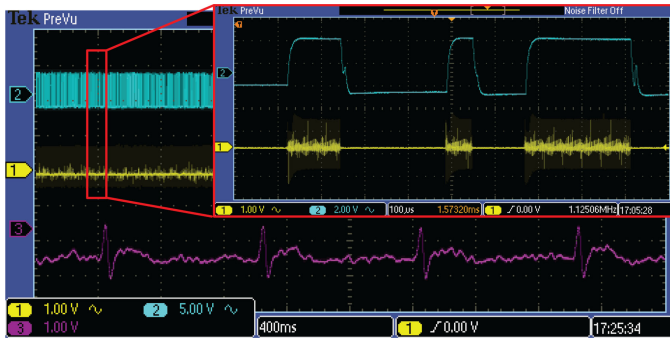


Fig. 19. Snapshots of signals in the HBC receiver (measured).

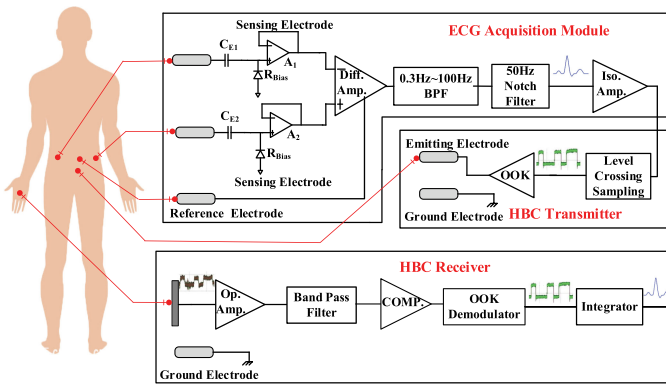


Fig. 20. Wearable ECG waist belt structure.

by the OOK demodulator. After that, the OOK output signals are either processed with an R-peak detection technique based on Kadane's algorithm or integrated to obtain the recovered ECG waveforms.

The R-peaks, as well as heart beat rates, can be detected from the Output 1 in Fig. 17. As shown in Fig. 21, the incremental parts of the P waves, R waves, S waves, and T waves can all trigger the uLCS. Since the R wave generally has the steepest slope and the most significant amplitude variation, it produces the most compact uLCS impulses during one QRS complex compared with other waveforms. Thus, the R-peaks can be detected by finding out the maximum subsequences in

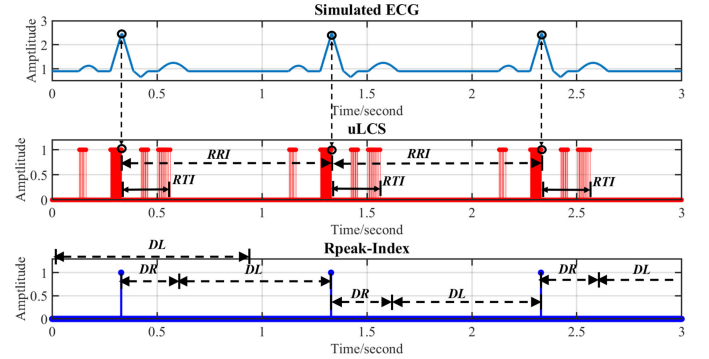


Fig. 21. R-peak detection principles (simulated).

the Output 1. Our R-peak detection algorithm uses Kadane's algorithm [25] as a computationally low-cost method to find the sum of the contiguous sub-array in a one-dimensional array with the largest sum. Since the LCS samples are a binary sequence, R-peaks can be extracted after LCS sampling with the Kadane's algorithm efficiently.

The algorithm is summarized in Algorithm 1. Line 3–15 scan from  $s[N]$  to  $s[N + DL * fs]$ . After the loop in line 3–15, one R-peak during  $DL$  (see Fig. 21) can be detected. Line 16 starts a new scan from  $s[k + DR * fs]$  to find the next R-peak until the end of the input sequence, where  $k$  is the position of the last R peak. Line 17 exports  $Rpeak\_Index$ , in which those elements equal to 1 represent the positions of R-peaks. The relationship between  $DR$  and  $DL$  is illustrated as in Fig. 21.

In general,  $DR$  is about  $0.15 \text{ s} \sim 0.3 \text{ s}$ , and  $DL$  is about  $0.8 \text{ s} \sim 1.1 \text{ s}$ .  $DR$  and  $DL$  satisfy

$$\begin{cases} RRI \leq DL + DR \leq 2RRI \\ RTI \leq DR \leq RRI \end{cases} \quad (3)$$

where  $RRI$  is the R-R interval and  $RTI$  is the R-T interval.

## IV. EXPERIMENTAL RESULTS

### A. Measurement Setup

The prototype apparatus is shown in Fig. 22. Two capacitively-coupled ECG sensing electrodes are fabricated on

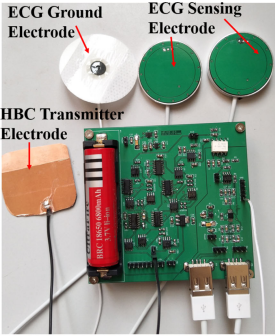


Fig. 22. The prototype apparatus.

**Algorithm 1:** R-Peak Detection Based On Kadane's Algorithm.
**Input:**

```

Input sequence  $s[1 : L]$ ;
The length of input sequence  $L$ ;
LCS clock frequency  $f_s$ ;
Output:
R-peak position index array,  $Rpeak\_Index$ ;
1:  $s[1 : L] = 2 \times s[1 : L] - 1$ 
2: Create variables  $k = 0$ ,  $N = 0$  and array
 $Rpeak\_Index[1 \dots L] = \{0 \dots 0\}$ 
3: Initialize  $ThisSum = 0$ ,  $MaxSum = 0$ 
4: for  $j = N$  to  $(N + DL \cdot f_s)$  do
5:    $ThisSum = ThisSum + s[j]$ ;
6:   if  $ThisSum > MaxSum$  then
7:      $MaxSum = ThisSum$ ;
8:      $Rpeak\_Index[j] = 1$ ;
9:      $k = j$ ;
10:     $Rpeak\_Index[1 \dots (j - 1)] = 0 \dots 0$ ;
11:   end if
12:   if  $ThisSum < 0$  then
13:      $ThisSum = 0$ ;
14:   end if
15: end for
16:  $N = k + DR$ , repeat line 3–16 until  $DL \cdot f_s + N > L$ .
17: return  $Rpeak\_Index$ ;

```

four-layer PCB with a diameter of 4 cm as in [17] and [22]. One commercially available Ag/AgCl electrode is attached to the abdomen skin as the ECG ground electrode. One copper electrode with an area of  $4 \text{ cm} \times 5 \text{ cm}$  is used as the HBC transmitter electrode. The ECG acquisition and the HBC transmitter circuits are fabricated on one PCB but isolated with an isolation amplifier. One circular electric potential electrode with 4-cm diameter is used as the receiver electrode. Both the HBC transmitter ground electrode and the receiver ground electrode remain floating. The copper pour on the circuit board serves as the ground electrode. The transmitter ground size is  $7 \text{ cm} \times 9 \text{ cm}$  and the receiver ground size is  $5 \text{ cm} \times 9 \text{ cm}$ .

Fig. 23 shows the experimental setup. The electrodes are woven under a waist belt that is fastened to the abdomen of a

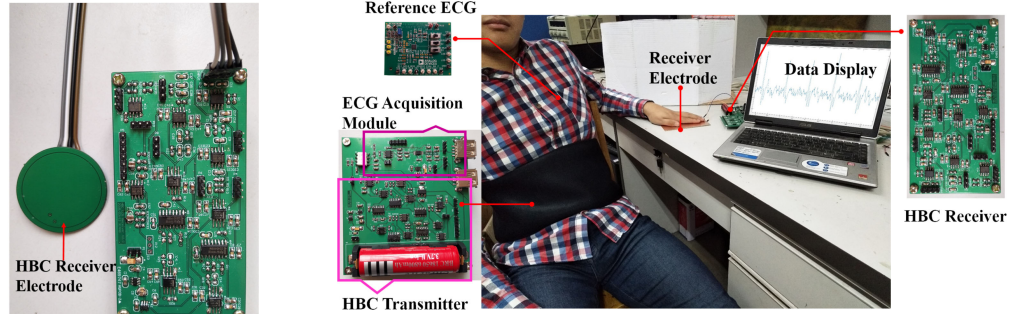
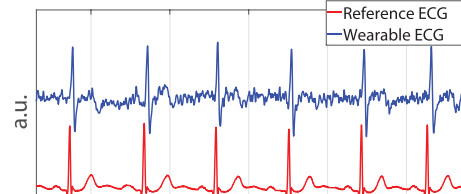
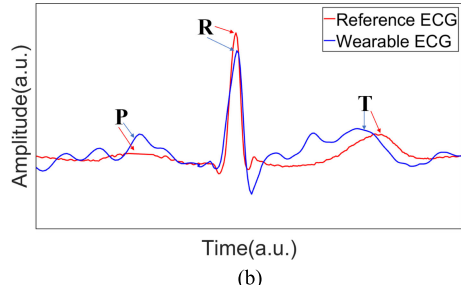


Fig. 23. Experiment setup for the wearable ECG waist belt.



(a)



(b)

Fig. 24. (a) acquired ECG signals (measured); (b) one aligned heart beat (measured).

23-year-old male on top of a thin cotton T-shirt. The person under test was asked to wear the belt and place his hand on the receiving electrode. Meanwhile, the reference ECG was measured from Ag/AgCl electrodes on the chest with a commercial ECG front end AD8232 (Analog Devices, Inc.).

### B. ECG Waveform Evaluation

The acquired ECG signals are shown in Fig. 24. The signal amplitude is normalized for comparison. The wearable ECG signal lagged behind the reference ECG signal on time axis, which is caused by the HBC transmission delay and time delay at receiver. In Fig. 24(b), the R-peak is aligned by shifting on time axis in order to gain a clear understanding of the correlation between the two ECG signals. Not only the QRS-wave but also the P-wave and T-wave are visible in the recovered ECG waveform. One reason for the morphology difference may be the configuration position of the electrodes. Another reason is that noncontact ECG electrodes are more susceptible to environmental noise such as power line interference compared with Ag/ACl electrodes. Therefore, the wearable ECG is a bit noisy.

Six volunteers (male, ranged from 23–30 years of age) were experimentally tested with the wearable ECG waist belt and

TABLE II  
COMPARISON OF *SDR* BETWEEN WEARABLE ECG AND REFERENCE ECG

	Subject1	Subject2	Subject3	Subject4	Subject5	Subject6
HBC ECG	0.46	0.47	0.45	0.49	0.39	0.41
Ref ECG	0.40	0.40	0.40	0.46	0.37	0.42
Diff(%)	15	17.5	12.5	6.5	5.4	2.4

TABLE III  
COMPARISON OF *Kur* BETWEEN THE PROPOSED WEARABLE ECG AND THE REFERENCE ECG

	Subject1	Subject2	Subject3	Subject4	Subject5	Subject6
HBC ECG	25.02	31.85	23.15	24.28	23.23	21.26
Ref ECG	29.99	26.47	21.53	27.01	29.90	26.71
Diff(%)	16.5	20.3	7.5	10.1	22.3	20.4

the reference ECG module simultaneously. They were asked to rest quietly on the chair for five minutes while acquiring data. No volunteers reported any difficulties or discomfort during experiments.

Spectral density ratio (SDR) and kurtosis value (Kur) are two widely used Signal Quality Indicators (SQIs) for ECG [26]. The SDR indicates the ratio of the power spectral density between 5 Hz and 15 Hz to the broader spectrum between 0.5 Hz and 50 Hz.

$$SDR = \frac{\int_5^{15} PSD}{\int_{0.5}^{50} PSD} \quad (4)$$

Kurtosis was calculated according to (5) [17]. Data with high kurtosis value tend to have distinct peaks near the mean. For ECG, Kur indicates the significance of the QRS complex.

$$Kur = \frac{\mu_4}{\sigma^4} - 3 = \frac{E(X - E(X))^4}{\{E(X - E(X))^2\}^2} - 3 \quad (5)$$

The statistical analysis was conducted for the six volunteers as shown in Table II and Table III. The relative difference of *SDR* ranges from 2.4% to 17.5% and the relative difference of *Kur* ranges from 7.5% to 22.3%. Although there are some individual differences, these results demonstrate that the HBC-based wearable ECG provides almost comparable performance as the reported papers [3], [17].

To validate the applicability of the wearable ECG in daily life usage, a healthy volunteer (male, 170 cm, 60 kg) was further experimentally tested during physical movements and respiration. The procedures were divided into five phases: 1. sitting (20 s) → 2. standing (30 s) → 3. sitting/breathing (60 s) → 4. apnea (30 s) → 5. breathing (30 s).

Fig. 25 shows one complete record of the measurement procedures. For capacitive ECG acquisition with noncontact electric field sensors, one drawback, as explained in [27], is their susceptibility to baseline drift that may attribute to the large setting time constant and displacement of the skin-electrode interface. However, in Fig. 26, no baseline was observed because after sampling by LCS, the baseline drift is removed. LCS is sensitive to event signals. For slowly changing baseline drifts, little or no samples are generated because they did not cross the levels. Thus, baseline drift that commonly presents in capacitive non-contact ECG is not obvious after LCS demodulation. The

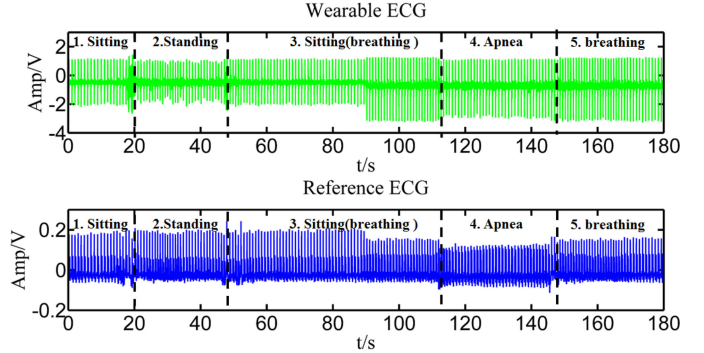


Fig. 25. One example of complete ECG record (measured).

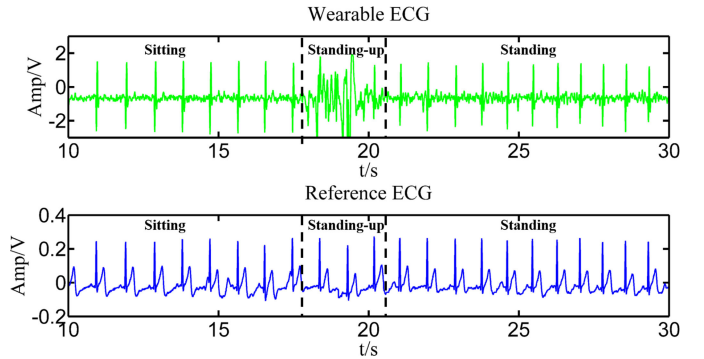


Fig. 26. Physical movements cause ECG corruption (measured).

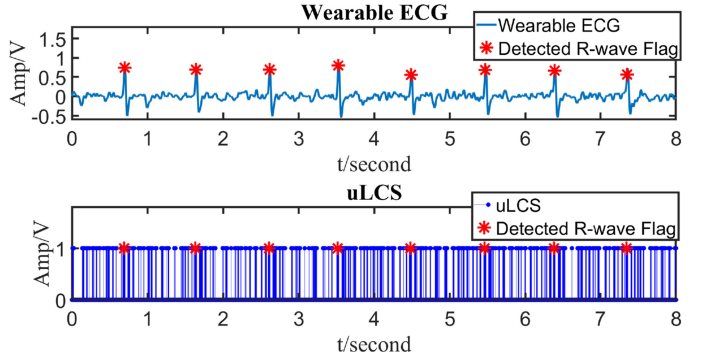


Fig. 27. Recovered ECG (top) and uLCS (bottom) at receiver (measured).

reference ECG in Fig. 26 has little baseline drift because of the wet and cohesive contact with the skin. The peaks of the QRS complex are clearly visible. During the transient duration of physical movements (see the sitting-to-standing and standing-to-sitting regions in Fig. 25), large motion artifacts appeared. In Fig. 26, the recorded wearable ECG signal is corrupted by motion artifacts for the standing-up duration. This was due to the variations of the coupling capacitance between the skin and the sensing electrodes caused by physical movements. When the movement stopped and the tested volunteer stood still, the wearable ECG signal restored to the normal state.

### C. R-peak Detection Evaluation

The R-peak detection algorithm proposed in Section III is evaluated by ECG records from the six volunteers (Section IV-B). Fig. 27 shows a time trace example of the R-peak

TABLE IV  
R-PEAK DETECTION EVALUATION

	Subject1	Subject2	Subject3	Subject4	Subject5	Subject6	Total
FN	3	4	2	1	9	2	21
FP	0	0	0	5	1	3	9
TP	325	345	310	300	440	360	2080
Se(%)	99.09	98.85	99.36	99.67	98.00	99.45	99.00
+P(%)	100	100	100	98.36	99.77	99.17	99.57
DER(%)	0.91	1.15	0.64	1.99	2.23	1.38	1.43

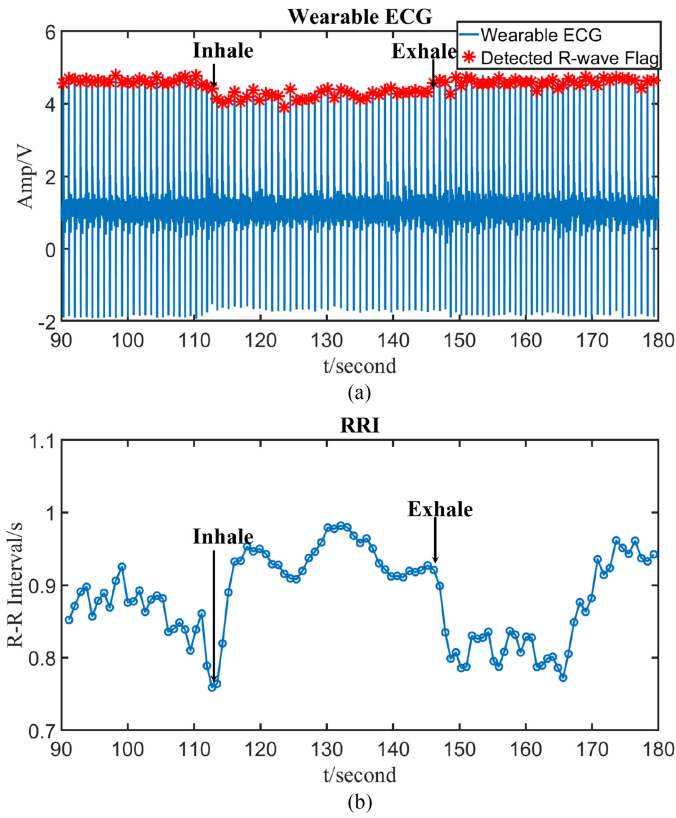


Fig. 28. Results of respiration experiment (measured).

detection results. The recovered ECG signals are obtained at the HBC receiver and the uLCS sequences are obtained from Output 1 (Fig. 17), where the detected R-peaks are indicated by star marks.

False negative (FN), false positive (FP), true positive (TP), sensitivity (Se), positive prediction (+P), and detection error (DER) are defined as in [11] to evaluate the performance of the R-peak detection algorithm. The true locations of the R-peaks are manually found from the recorded signals to be used as the reference. The results are summarized in Table IV, indicating a positive prediction of 99.57%, a sensitivity of 99.00%, and a detection error of 1.43%. This performance is comparable to the current R-peak detection algorithm in [18] and [11].

It is well-known that the respiration effort has great influence on heartbeat rate. The experiment during 90 ~ 180 s in Fig. 28 is designed to simulate the Valsalva maneuver experiment. As shown in Fig. 28, clear QRS complexes can be obtained during the experiment. The R-R intervals are calculated by the detected R-peaks (see Fig. 28b). When the volunteer started to inhale deeply, the R-R interval began to increase sharply. After a short

while, the R-R interval decreased slightly but oscillated upward slowly later on. After exhaling, the R-R interval dropped down dramatically and then underwent a great vibration period. The results are in accordance with [28].

#### D. Power Consumption Evaluation

The total power consumption of each module in the prototype system, including ECG acquisition, level crossing sampling, and HBC data transmission, are tested. The circuits are powered by 3.7 V 18650 lithium-ion rechargeable batteries with a large capacity of 4000 mAh. In Fig. 20, the ECG acquisition module, the HBC transmitter module, and the HBC receiver module are powered by batteries separately. Low-power DC/DC voltage converters PTN04050A and PTN04050C, which have high efficiency up to 90%, are used to provide +5 and -5 V supply.

During the test, all modules are powered on and in active mode. The power consumptions are computed by the product of the voltages and the currents measured at the output of the corresponding batteries. The HBC transmission power is measured at the transmitter electrode. We tested the AC voltage of the transmitter electrode and then inserted an ammeter in series (in-line) with the output of OOK to get the AC current. By subtracting the power of the HBC transmission from the sum power of the battery, we got the power consumption of LCS module.

Table V summarizes the comparison of power consumption between our work and other similar studies. As it is indicated, the power consumption of our capacitive HBC is 0.53 nJ/b, which is lower than that of ANT, ZB, and BLE [31]. The result demonstrates that capacitive HBC is a more efficient scheme for wireless data transmission than the prevalent protocols, which has been confirmed by other studies [5], [6] as well. The power consumption of our ECG acquisition module is lower than similar studies implemented with COTS [1], [29]. The reason is that, instead of using dual supply and high power consumption chips like INA116 ( $\pm 5$  V, 1.4 mA typical) [1] and OPA27 ( $\pm 5$  V, 3.3 mA typical) [29], we use +5 V single supply micropower instrumentation amplifier INA122 (60  $\mu$ A typical) for front-end differential amplification and micropower OPA2333 (17  $\mu$ A typical) for bandpass and notch filter. On the other hand, the level crossing sampling module has significant larger power consumption compared with other CMOS-based studies [13]–[15]. This is reasonable because our work is implemented with discrete COTS components. Our approach is primarily intended to provide a proof-of-concept demonstration of the proposed LCS scheme. It is expected that the power consumption could be greatly reduced if the proposed system is realized in CMOS process as [32]. As for the HBC receiver, it consumes 115.5 mW. Since the HBC receiver is not integrated into the wearable waist belt, it is less constrained by power supply and therefore it is not listed in Table V and not compared with other studies.

#### E. HBC Performance

Table VI summarizes the performance of the proposed HBC compared with previous studies. Our proposed HBC has the lowest operation frequency (from 100 kHz to 1 MHz) and the lowest HBC loss (10 dB loss at 1 MHz, 120 cm) with only

TABLE V  
POWER CONSUMPTION EVALUATION

Ref.	ECG acquisition				Level crossing sampling				Data transmission			
	[29]	[1]	[30]	Ours	[13]	[14]	[15]	Ours	[31]	[31]	[31]	Ours
Volt.(V)	$\pm 5$	3	3	<b>3.7</b>	1	1	1.8–2.4	<b>3.7</b>	3.3	3.3	3.3	<b>3.7</b>
Power	116mW	75 mW	12.5mW	25mW	8.49 $\mu$ W	402 $\mu$ W	0.6–2.0 $\mu$ W	<b>126mW</b>	<b>4</b> $nJ/b$	<b>4</b> $nJ/b$	<b>4</b> $nJ/b$	<b>0.53</b> $nJ/b$
Tech.	COTS	COTS	CMOS	<b>COTS</b>	CMOS	CMOS	CMOS	<b>COTS</b>	ANT	BLE	ZB	<b>HBC</b>

TABLE VI  
HBC PERFORMANCE SUMMARY AND COMPARISON

Ref.	[3]	[5]	[6]	[4]	Ours
Frequency	10-60 MHz	500 kHz	145-433 MHz	1-100 MHz	100 kHz-1 MHz
Receiver electrode	metallic electrode	metallic electrode	Ag/AgCl	PCB plane	electric field sensor
Modulation	IR OOK	none	OOK	none	OOK
Data Rate	1.25Mb/s	500kb/s	2Mb/s	5Mb/s	15kb/s
Power Consumption	3.84nJ/b	9.4nJ/b	2.27 nJ/b	0.164 nJ/b	0.53nJ/b
Technology	COTS	COTS	CMOS	CMOS	COTS
HBC Path Loss	70-80 dB attenuation at 30 MHz from the chest to a fingertip (around 90 cm)	37.3 dB attenuation at 500 kHz wide-band signaling from the wrist to elbow (around 30 cm)	About -7 dB loss from 50 to 300 MHz, from forearm to wrist (around 30 cm)	About 80 dB attenuation at 1 MHz, 15 cm	10 dB attenuation at 1 MHz, 120 cm

0.53 nJ/b power consumption. The power consumption is lower than other similar COTS system [3], [5], and even lower than some CMOS implemented system [6]. One reason is that our system working in sub-megahertz from 100 kHz to 1 MHz consumes much fewer energy than those working up to tens of megahertz. Because as pointed out by [33], the dynamic power dissipation is about linearly proportional to the working frequency. Moreover, a further reduction on the path loss of capacitive HBC could result in even lower power consumption [34]. The body channel is enhanced by more than 30 dB with the proposed method. It would be more power efficient because less emission power is required for HBC transmission. Even though the data rate of the proposed HBC is only 15 kb/s, it is adequate for biomedical signal sampling. By using COTS parts with larger bandwidth, the proposed HBC can extend the operation frequency to achieve higher data rate if necessary.

## V. CONCLUSION

Data compression and wireless transmission are two essential problems for wearable sensors. The main focus of our work is combining HBC with LCS to develop a wearable ECG waist belt. Using a high input impedance electric field sensor as the HBC receiver electrode, the HBC operation frequency is greatly reduced to 100 kHz-1 MHz. The experimental results validated that the proposed wearable ECG waist belt performs a good agreement with regular Ag/AgCl attachment acquisition method. Because the LCS is only sensitive to the spike-like signals, the slowly varying baseline shifting can be suppressed. For heartbeat detection with a technique using the Kadane's algorithm, Se of 99.00%, +P of 99.57% and DER within 1.43% are obtained.

Wearable sensors employing LCS and HBC have many potential applications. LCS is suited for sparse biomedical signals such as the QRS complex of ECG, muscle contraction potentials of EMG, or neural action potentials (spikes) of EEG. The target applications fall into two categories. One application is used as a single wearable ECG device. For example, ref [3] examined the feasibility of HBC-based wearable ECG for car drivers. In this scenario, the user wears the wearable belt and places his hands on the steering wheel, from where the ECG signals are continuously transmitted to an off-body receiver. One limitation of this configuration is that placing the hand on the receiver electrode is not convenient or even not allowed in some cases. Another category of application is arranging various biomedical sensors on the human body, not just an ECG sensor. In this scenario, LCS is utilized as an efficient sampling method and the HBC receiver serves as the communication hub on the body to collect multiple vital data on the human body. The HBC hub is configured on the body to aggregate all the data and then send to a remote station through a wireless medium or through HBC when the user touches an electrode in the human-machine interaction [5]. Our system has demonstrated the feasibility of a single ECG sensor in the BSN framework of combining LCS and HBC. This will pave way for LCS-HBC based BSN system.

## REFERENCES

- [1] E. Nemati, M. J. Deen, and T. Mondal, "A wireless wearable ecg sensor for long-term applications," *IEEE Commun. Mag.*, vol. 50, no. 1, pp. 36–43, Jan. 2012.
- [2] J. Li, Y. Liu, Z. Nie, W. Qin, Z. Pang, and L. Wang, "An approach to biometric verification based on human body communication in wearable devices," *Sensors*, vol. 17, no. 1, 2017, Art. no. 125.

- [3] J. Wang, T. Fujiwara, T. Kato, and D. Anzai, "Wearable ecg based on impulse-radio-type human body communication," *IEEE Trans. Biomed. Eng.*, vol. 63, no. 9, pp. 1887–1894, Sep. 2016.
- [4] K. Lin, B. Wang, X. Zhang, X. Wang, T. Ouyang, and H. Chen, "A novel low-power compact wbs human body channel receiver for wearable vital signal sensing application in wireless body-area network," *Microsystem Technol.*, vol. 23, no. 10, pp. 4459–4473, 2017.
- [5] S. Maity, D. Das, and S. Sen, "Wearable health monitoring using capacitive voltage-mode human body communication," in *Proc. 39th Annu. Int. Conf. IEEE Eng. Med. Biol. Soc.*, 2017, pp. 1–4.
- [6] Y.-T. Lin, Y.-S. Lin, C.-H. Chen, H.-C. Chen, Y.-C. Yang, and S.-S. Lu, "A 0.5-v biomedical system-on-a-chip for intrabody communication system," *IEEE Trans. Ind. Electron.*, vol. 58, no. 2, pp. 690–699, Feb. 2011.
- [7] S. Maity, D. Das, X. Jiang, and S. Sen, "Secure human-internet using dynamic human body communication," in *Proc. IEEE/ACM Int. Symp. Low Power Electron. Design*, 2017, pp. 1–6.
- [8] R. Kumar, A. Kumar, and R. K. Pandey, "Beta wavelet based ecg signal compression using lossless encoding with modified thresholding," *Comput. Electr. Eng.*, vol. 39, pp. 130–140, 2013.
- [9] L. F. Polania, R. E. Carrillo, M. Blanco-Velasco, and K. E. Barner, "Exploiting prior knowledge in compressed sensing wireless ecg systems," *IEEE J. Biomed. Health Informat.*, vol. 19, no. 2, pp. 508–519, Mar. 2015.
- [10] G. D. Poian, C. J. Rozell, R. Bernardini, R. Rinaldo, and G. D. Clifford, "Matched filtering for heart rate estimation on compressive sensing ecg measurements," *IEEE Trans. Biomed. Eng.*, vol. 65, no. 6, pp. 1349–1358, Jun. 2018.
- [11] N. Ravanshad, H. Rezaee-Dehsorkh, R. Lotfi, and Y. Lian, "A level-crossing based qrs-detection algorithm for wearable ecg sensors," *IEEE J. Biomed. Health Informat.*, vol. 18, no. 1, pp. 183–192, Jan. 2014.
- [12] R. Rieger and J. T. Taylor, "An adaptive sampling system for sensor nodes in body area networks," *IEEE Trans. Neural Syst. Rehabil. Eng.*, vol. 17, no. 2, pp. 183–189, Apr. 2009.
- [13] Y. Li, A. Mansano, Y. Yuan, D. Zhao, and W. A. Serdijn, "An ecg recording front-end with continuous-time level-crossing sampling," *IEEE Trans. Biomed. Circuits Syst.*, vol. 8, no. 5, pp. 626–635, Oct. 2014.
- [14] J. Zhou *et al.*, "Compressed level crossing sampling for ultra-low power iot devices," *IEEE Trans. Circuits Syst. I, Reg. Papers*, vol. 64, no. 9, pp. 2495–2507, Sep. 2017.
- [15] T. Marisa *et al.*, "Pseudo asynchronous level crossing adc for ecg signal acquisition," *IEEE Trans. Biomed. Circuits Syst.*, vol. 11, no. 2, pp. 267–278, Apr. 2017.
- [16] R. Agarwal and S. R. Sonkusale, "Input-feature correlated asynchronous analog to information converter for ecg monitoring," *IEEE Trans. Biomed. Circuits Syst.*, vol. 5, no. 5, pp. 459–467, Oct. 2011.
- [17] B. Yang, C. Yu, and Y. Dong, "Capacitively coupled electrocardiogram measuring system and noise reduction by singular spectrum analysis," *IEEE Sensors J.*, vol. 16, no. 10, pp. 3802–3810, May 2016.
- [18] V. P. Rachim and N. T. Hau, "Wearable noncontact armband for mobile ecg monitoring system," *IEEE Trans. Biomed. Circuits Syst.*, vol. 10, no. 6, pp. 1112–1118, Dec. 2016.
- [19] J. Bae, H. Cho, K. Song, H. Lee, and H.-J. Yoo, "The signal transmission mechanism on the surface of human body for body channel communication," *IEEE Trans. Microw. Theory Techn.*, vol. 60, no. 3, pp. 582–593, Mar. 2012.
- [20] M. D. Pereira, G. A. Alvarez-Botero, and F. R. de Sousa, "Characterization and modeling of the capacitive HBC channel," *IEEE Trans. Instrum. Meas.*, vol. 64, no. 10, pp. 2626–2635, Oct. 2015.
- [21] S. Maity, K. Mojabe, and S. Sen, "Characterization of human body forward path loss and variability effects in voltage-mode hbc," *IEEE Microw. Wireless Compon. Lett.*, vol. 28, no. 3, pp. 266–268, Mar. 2018.
- [22] A. J. Portelli and S. J. Nasuto, "Design and development of non-contact bio-potential electrodes for pervasive health monitoring applications," *Biosensors*, vol. 7, no. 1, 2017, Art. no. 2.
- [23] Ž. Lucev, I. Krois, and M. Cifrek, "A capacitive intrabody communication channel from 100 khz to 100 mhz," *IEEE Trans. Instrum. Meas.*, vol. 61, no. 12, pp. 3280–3289, Dec. 2012.
- [24] M. Miskowicz, "Send-on-delta concept: an event-based data reporting strategy," *Sensors*, vol. 6, no. 1, pp. 49–63, 2006.
- [25] M. A. Weiss, *Data Structures and Algorithm Analysis in C*. San Francisco, CA, USA: Benjamin/Cummings California, 1993.
- [26] I. D. Castro, M. Mercuri, T. Torfs, I. Lorato, R. Puers, and C. V. Hoof, "Sensor fusion of capacitively coupled ecg and continuous-wave doppler radar for improved unobtrusive heart rate measurements," *IEEE J. Emerg. Sel. Topics Circuits Syst.*, vol. 8, no. 2, pp. 316–328, Jun. 2018.
- [27] Y. M. Chi, T.-P. Jung, and G. Cauwenberghs, "Dry-contact and noncontact biopotential electrodes: Methodological review," *IEEE Rev. Biomed. Eng.*, vol. 3, pp. 106–119, Oct. 2010.
- [28] B. Yang, Y. Dong, Z. Hou, and X. Xue, "Simultaneously capturing electrocardiography and impedance plethysmogram signals from human feet by capacitive coupled electrode system," *IEEE Sensors J.*, vol. 17, no. 17, pp. 5654–5662, Sep. 2017.
- [29] D. Svard, A. Cichocki, and A. Alvandpour, "Design and evaluation of a capacitively coupled sensor readout circuit, toward contact-less ecg and eeg," in *Proc. Biomed. Circuits Syst. Conf.*, 2010, pp. 302–305.
- [30] F. Miao, Y. Cheng, Y. He, Q. He, and Y. Li, "A wearable context-aware ecg monitoring system integrated with built-in kinematic sensors of the smartphone," *Sensors*, vol. 15, no. 5, pp. 11465–11484, 2015.
- [31] N. At, H. Senel, and R. S. M. Daraghma, "Multi-hop efficient protocol for zigbee, bluetooth low-energy and ant sensor nodes," *JCP*, vol. 13, pp. 471–479, 2018.
- [32] X. Zhang and Y. Lian, "A 300-mv 220-nw event-driven adc with real-time qrs detection for wearable ecg sensors," *IEEE Trans. Biomed. Circuits Syst.*, vol. 8, no. 6, pp. 834–843, Dec. 2014.
- [33] N. S. Kim *et al.*, "Leakage current: Moore's law meets static power," *IEEE Comput.*, vol. 36, no. 12, pp. 68–75, Dec. 2003.
- [34] J. Mao, H. Yang, and B. Zhao, "An investigation on ground electrodes of capacitive coupling human body communication," *IEEE Trans. Biomed. Circuits Syst.*, vol. 11, no. 4, pp. 910–919, Aug. 2017.

**Jinxi Xiang** received the B.S. degree from Wuhan University, Wuhan, China, in 2016. He is currently working toward the Ph.D. degree with Tsinghua University, Beijing, China. His main research interests include wearable devices, electrical field sensors, and magnetic induction sensors.

**Yonggui Dong** received the B.S. degree in mechanical engineering and the Ph.D. degree in mechatronics from Tsinghua University, Beijing, China, in 1988 and 1994, respectively. He is currently a Professor and Ph.D. Supervisor with the Department of Precision Instruments, Tsinghua University. His current research interests include sensor technology, measurement and test technology, and intelligent instruments technology.

**Xiaohui Xue** was born in Xingtai, China, in 1994. He is currently working toward the Ph.D. degree with Tsinghua University, Beijing, China. His main research interest includes human vital signal measuring.

**Hao Xiong** received the B.Sc. degree from the University of Science and Technology, Beijing, China, in 2013. He is currently working toward the Ph.D. degree with Tsinghua University, Beijing, China. His main research interest includes sensing coil measurement.